Electronic structure of double perovskite Pr_2MnNiO_6 from core-photoemission and density functional theory.

Padmanabhan Balasubramanian [1,2], Shalik Ram Joshi[2], Ruchika Yadav[3], Frank M. F. de Groot[4], Amit Kumar Singh[5], Avijeet Ray[1], Mukul Gupta[6], Ankita Singh[1], Suja Elizabeth[3], Shikha Varma[2] Tulika Maitra[1] ‡,Vivek Malik [1]

[1]**Department of Physics, Indian Institute of technology, Roorkee-247667, Uttarakhand, India.**
[2]**Institute of Physics, Bhubaneshwar-750012, India**
[3]**Department of Physics,Indian Institute of Science, C.V. Raman Avenue, Bangalore-560012, India**
[4]**Inorganic Chemistry Catalysis, Debye Institute for Nanomaterials Science, Utrecht University, Universiteitsweg 99, Utrecht 3584 CG, The Netherlands**
[5]**Institute Instrumentation Centre, Indian Institute of technology, Roorkee-247667, Uttarakhand, India.**
[6]**UGC-DAE Consortium for Scientific Research, University Campus, Khandwa Road, Indore 452 017, India.**

Abstract. Electronic structure of double perovskite Pr_2MnNiO_6 is studied using core x-ray photoelectron spectroscopy and absorption spectroscopy. The $2p$ absorption spectra clearly shows that Mn and Ni are in 2+ and 4+ states respectively. Using charge transfer multiplet theory analysis of Ni and Mn $2p$ XPS spectra, we find reduced charge transfer energy Δ of 3.5 and 2.5 eV for Ni and Mn respectively. In addition, we find a larger hybridization of Ni and Mn $3d$ orbitals with the O $2p$ orbitals. The ground state of Ni^{2+} and Mn^{4+} reveal a much higher d electron count of 8.21 and 3.38 respectively, indicating the covalent nature of the system. The O K edge absorption spectra reveal a band gap of 0.8 eV which is comparable to the value obtained from first principle calculations for $U-J > 0$. The density of states clearly reveal a strong p-d type charge transfer character of the system, with band gap proportional to average charge transfer energy of Ni^{2+} and Mn^{4+}.

Double perovskites; Ferromagnetism, photoemission spectroscopy, density of states

‡ tulimfph@iitr.ac.in, tel: 91-1332-285764.

1. Introduction

Transition metal compounds have always been of great interest since they show diverse physical properties like metal-insulator transition, high temperature superconductivity, multiferroicity and various interesting phenomena like charge/orbital ordering and complex magnetic ordering. These systems include simpler oxides and halides like NiO, CuF_2, MnO or more complex materials like perovskite structured rare-earth manganites, cuprates and nickelates. In most cases the parent compound is insulating, which becomes metallic under influence of doping, pressure and so on. In a unified scenario, insulating nature in the various oxides(along with sulphides, dihalides etc) can be described by the Zannen-Sawatzky-Allen(ZSA) phase diagram which classifies the materials into Mott-Hubbard and charge-transfer insulators[1]. The electronic behaviour is governed mainly by three parameters namely $d-d$ Coulomb repulsion U_{dd} in the metal ion, ligand to metal charge transfer energy Δ and and metal-ligand hybridization strength V_{pd}[1]. In the early transition metal compounds, (Ti, V and Cr based compounds), $U_{dd}<\Delta$, due to which the bandgap $E_g \propto U_{dd}$ in which case, the materials are known as Mott-Hubbard insulators. Some of the late transition metal based compounds(eg: hole doped cuprates, $NiCl_2$,$NiBr_2$), show greater ligand-metal charge transfer and for which $U_{dd}>\Delta$. Their band gap $E_g \propto \Delta$, due to which these materials are known as charge transfer insulators. In a charge transfer insulator, the ground state involves a strong fluctuation between d^n and $d^{n+1}L$ states where L is the ligand hole. However in compounds involving Mn and Fe, the scenario is much more complicated and the band gap can be considered of an intermediate character. In addition to ratios, U_{dd}/V_{pd} and Δ/V_{pd}, additional parameters like $3d$ bandwidth W and anion bandwidth w play an important role in determining whether the given compound is a metal or insulator.

$2p$ x-ray core-level photoemision and absorption spectroscopy are two powerful probes of the various interaction strenghts. Appearance of prominent satellite peaks in the core XPS spectra help in determining the three parameters using cluster analysis or single impurity Anderson model[2]. The position and intensity of the satellite peaks systematically depend on the surrounding ligand which is an indicator of strength of covalency, related directly to the transfer integrals $V_{pd\sigma}$ and $V_{pd\pi}$. The core XPS spectra also reveal the role of charge transfer in a very obvious manner in the late transition metal compounds, the spectra being extremely sensitive to Δ and electronegativity of the anion [3]. However the XPS spectra is severely broadened by multiplet structure and the core hole. Complementary to XPS is the $2p$ XAS technique, which has certain advantages over XPS. Depending on the valency of the metal, the $2p$ XAS spectra has a distinct shape. Also unlike XPS, which accesses the full multiplet, the no of transitions are restricted by the dipole transition rules.

Core level XPS and XAS studies have been carried out in-depth on the nickelates($RNiO_3$) and manganites($RMnO_3$) in great detail. In the nickelates, studies have shown the variation of covalency and reduced hopping as we go from La to Nd,[4] causing changes in conducting behaviour. The Ni ion due to its high valence state of 3+ has a very small charge transfer energy ($\Delta \sim 1$ eV) leading to metallicity or an insulator with a very small band gap. On the other hand, the parent manganite compounds posseses a larger band gap which have entirely different origins. In $RMnO_3$ (R = La, Pr, Nd) the band gap arises due to the Jahn-Teller at the Mn^{3+} site, while in $CaMnO_3$ which is an Mn^{4+} system, the gap arises due to the large crystal field splitting[5]. In $RMnO_3$, the ground state shows a larger % of d^4 and a smaller %

of d^5L states with $\Delta\sim$4-5 eV. However in (Ca/Sr)MnO_3, with a smaller $\Delta\sim$3 eV as seen from valence band and $2p$ core level photoemission[6] is considered as a charge transfer insulator.

However, the homovalent substitution of Mn and Ni as in in $LaMn_{1-x}Ni_xO_3$ leads to totally different ground state, especially for x = 0.5. The half doped compound, $LaMn_{0.5}Ni_{0.5}O_3$ also crystallizes as La_2MnNiO_6. The former is orthorhombic($Pbnm$) while the latter belongs to the class of double perovskite compounds with monoclinic symmetry. In the orthorhombic structure, Mn and Ni ions are randomly arranged, since they occupy the same Wycoff positon $2b$. However charge disproportionation results in formation of Mn^4 and Ni^{2+} by the following reaction, Ni^{3+}+Mn^{3+} $\rightleftharpoons$ Ni^{2+}+Mn^{4+}[7, 8]. This favours a rocksalt like arrangement of Mn and Ni resulting in monoclinic double perovskite compound La_2MnNiO_6. Our studies are based on the double perovskite material Pr_2MnNiO_6, which is relatively less explored. The parent compounds, $PrMnO_3$ and $PrNiO_3$, which are more complex-ordered antiferromagnetic insulators, while Pr_2MnNiO_6 is a ferromagnetic insulator. The Mn^{4+}-Ni^{2+} super-exchange interactions which are ferromagnetic in nature, with a transition temperature, as high as 280 K in La_2MnNiO_6 [9]. With decreasing cationic radii due to increasing R, the decrease in <Mn-O-Ni> bond angle affects the exchange interaction and decreases the magnetic transition temperature. However even in perfectly ordered monoclinic structure, there occurs small percentage of randomness in distribution of Mn and Ni which are called as anti-site disorders. This result in Mn^{4+}-Mn^{4+} and Ni^{2+}-Ni^{2+} super-exchange interactions which are anti-ferromagnetic in nature. In the extreme limit of anti-site disorders, there occurs formation of Mn^{3+} and Ni^{3+} regions, which can result in Mn^{3+}-Ni^{3+}-ferromagnetic super-exchange interactions, resulting in second transition at lower temperature[7, 10]. Using $3s$ XPS, one can probe the valence state of Mn with greater precision, since the $3s$ splitting is proportional to the local spin of the Mn ion[11].

Irrespective of presence of anti-site disorders, even in the perfectly ordered Pr_2MnNiO_6, the resultant local electronic structure is different from both parent compounds. The combined overlap of Mn-O and Ni-O orbitals would affect the values of Δ, U_{dd} and V_{pd}. Thus it would be interesting to obtain an estimate of these parameters which lead to the ferromagnetic super-exchange interaction and also determine the band gap. This can also help us in obtaining precise nature of the conducting behaviour/band gap, according to the ZSA phase diagram. In the present paper we have used core level XPS and XAS accompanied by cluster-model calculations we have investigated the electronic structure of double perovskite Pr_2MnNiO_6. In addition, the O K edge XAS spectra was also obtained and compared with unoccupied density of states obtained using density functional theory.

2. Experimental

The polycrystalline samples of Pr_2NiMnO_6 a were synthesized by conventional solid-state reaction. Details of sample synthesis and characterization are discussed elsewhere. Zero field resistivity studies were carried out in temperature range of 4 to 300 K.Magnetic properties were measured using a superconducting quantum interference device (SQUID) in the temperature range 10 - 300 K. AC susceptibility measurements were carried out in a commercial CYROBIND set-up in the temperature range 4.2 - 280 K. XPS studies were carried out using Al Kα source with a hemisphere analyzer

with a resolution of 0.5 eV. The binding energies were calibrated w.r.t C 1*s* photoelectron line with binding energy of 284.6 eV . The spectra was collected at the Mn and Ni *2p*, *3s* edges along with the O *1s*. The XAS studies were carried out at BL-01 beamline in INDUS synchrotron centre, India at room temperature. The spectra was obtained at O K edge, Mn and Ni L edges using the total electron yield method. The resolution of spectra was 0.1 eV.

3. Computational

Computational studies were performed using the projector augmented wavefunction (PAW) method within the density functional theory. The ab-initio simuation package (VASP) was used for this purpose. The calculations were performed on PNNO for understanding of the electronic band structure and its impact on its magnetic and electrical properties. The Pr 5d, Mn 3d/4s, Ni 3d/4s, O2s O2p are considered as valence orbitals while the Pr $4f$ orbitals are considered as core levels. The calculations were performed within the generalized gradient approximation(GGA) formalism.Both GGA and GGA+U formalism was used to see the effect of exchange and correlations[12]. The plane wave basis was used with a cutoff of 600 eV. Gaussian broadening of 0.05 was used. Initially the crystal structure was relaxed until the forces on the atoms are less than 0.05 eV/ . The structural optimisation was carried out assuming a ferromagnetic ordering between the Mn and Ni spins in accordance with experiments. Then the selfconsistent electronic calculations were performed till the energy difference between successsive cycles were less than 10^{-5} eV. The band structure was obtained along specific directions along the Brillouin zone, while the partial spin polarized density of states were obtained by performing integrations using a 7 x7 x5 Monkhorst pack.

4. Results and discussion

The x-ray powder diffraction data of Pr_2MnNiO_6 was refined to monoclinic space group $P2_1/n$. The structural parameters obtained from our refinement are a = 5.4672Å b = 5.5362Å and c = 7.7336Å with $\beta = 89.88°$. The average Mn-O and Ni-O bondlengths are 1.93 and 2.04Å respectively. The parameters are well in agreement with the values reported[9]. The three Mn-O and Ni-O bond lengths are almost equal indicating absence of any octahedral disortions. The bond valence sums of 3.13 and 2.2 are nearly equal to the valencies expected from Mn^{4+} and Ni^{2+} system. Fig.1 shows plot of resistivity vs. temperature of Pr_2MnNiO_6. The plot is shown only till 160 K since the values of resisitivity went beyond the instrument range. Our material is insulating with an activation energy of 0.3 eV. The smaller value of activation energy is in agreement with the predicted band gap as obtained from DFT calculations as we would discuss below. Fig.2 shows magnetization plots of Pr_2MnNiO_6 for ZFC and FC cooling. The paramagnetic-ferromagnetic transition occurs at 210 K which arises due to O^{2-} mediated Mn^{4+}-Ni^{2+} super-exchange interactions. Absence of a second transition in our system indicates a very low concentration of anti-site disorder.The magnetic moment of Pr_2MnNiO_6 at 15 K and 5 T is around 4.8 μ_B which is close to the expected value of 5 μ_B due to perfectly ordered system. However the reduction and lack of saturation suggest presence of small amount of anti-site disorders, in addition to role of Pr^{3+} spins.

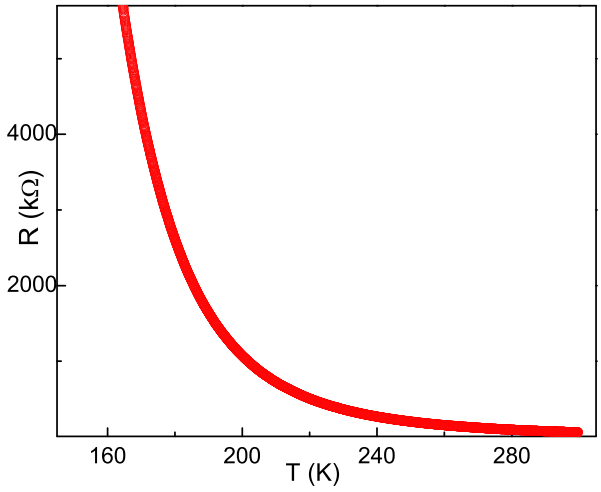

Figure 1. *Temperature dependenence of resisitance of Pr_2NiMnO_6.*

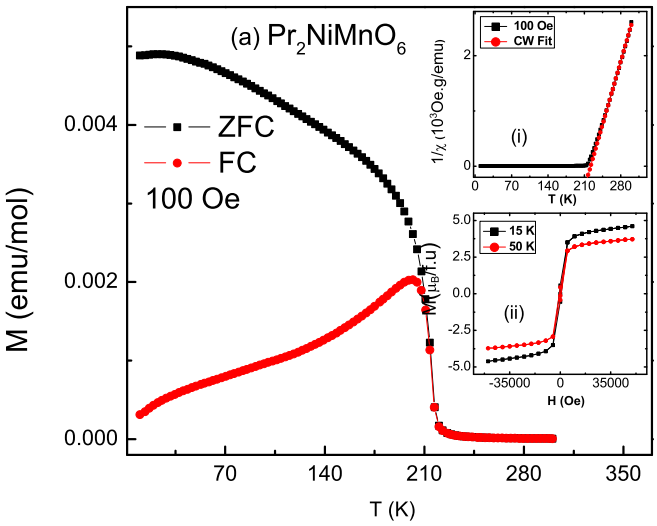

Figure 2. *ZFC-FC magnetization of Pr_2MnNiO_6 in a field of 100 Oe. The top inset shows inverse susceptibility vs temperature and the corresponding Curie-Weiss fitting. The lower inset shows the M vs H at 15 K and 50 K.*

4.1. XPS and XAS spectra

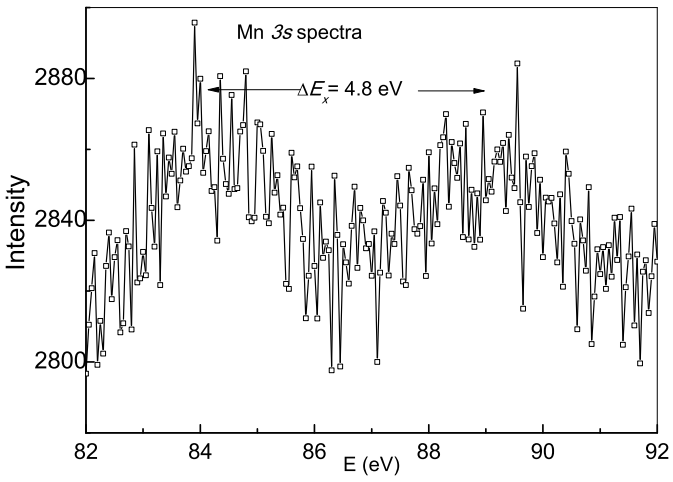

Figure 3. *Mn 3s XPS spectrum of Pr_2NiMnO_6 where the two peaks indicate exchange splitting.*

4.1.1. Mn 3s spectra The role of anti-site disorders in affecting the total magnetic moment is obtained more precisely from Mn 3s XPS spectra. The 3s spectra arises due to transition from the initial $|3s^2, 3d^3>$ to $|3s^1, 3d^3>$ states. The Mn 3s spectra shown in fig.3 exhibits a characteristic doublet which arises entirely due to the exchange splitting. This scenario is valid only in the case of early transition metal ions. In the case of Ni 3s, the effects of charge transfer reduces the observed exchange splitting. The difference between interaction of 3s electron with the parallel and anti-parallel spin states of the $3d^n$ shell gives rise to the exchange splitting. The magnitude of splitting is proportional the Slater exchange integral $G^2(3s,3d)$ which is given by Van-Vleck theorem as[13],

$$\hat{\Delta}E_{ex} = \left(\frac{(2S+1)G^2(3s,3d)}{2l+1}\right), \tag{1}$$

where l=2. The magnitude of ΔE_{ex} increases with decreasing valency. Our experimental spectra reveals an exchange splitting of nearly 4.8 eV. Assuming that $G^2(3s,3d)/(2l+1) = 1.1$ eV,the above equation yields a net spin of S=1.68. For an complete Mn^{4+} system like $CaMnO_3$, the value of E_x is nearly 4.5 eV[11], which yields a spin of $S = 3/2$. Thus in our material the value of S is very close to the expected spin value of $S = 3/2$ in an Mn^{4+} system. The slightly higher value of S, indicates presence of Mn^{3+} ions arising due to anti-site disorders. However the signature of Mn^{3+} is not so evident from our Mn 2p XPS and XAS spectra.

4.1.2. Simulation of Ni and Mn 2p XPS and XAS spectra In this section,we briefly discuss the theoretical simulation of the 2p XPS and XAS spectra. The simulations was done in the configuration interaction cluster model, using charge transfer multiplet program CTM4XAS[14]. The simulations were performed for a single ion of Ni^{2+} and

Mn^{4+} surrounded by oxygen ligand octahedra in O_h symmetry. The ground state electron configuration of Ni^{2+} is d^8, which in O_h symmetry is written as ${}^3A_{2g}(t_{2g}^6 e_g^2)$. We consider two charge transfer configurations, d^9L and $d^{10}L^2$, where L corresponds to a ligand hole in the O $2p$ state. The Mn^{4+} ion has d^3 configuration in ground state, which is written as ${}^4A_{2g}(t_{2g}^3)$ in O_h symmetry. The calculation of Mn $2p$ spectra involving two charge transfer configurations is computationally difficult. Hence we consider only the d^4L configuration in this case, also since effects of the d^5L^2 is not so prominent. The ground state wavefunctions for Ni^{2+} and Mn^{4+} ions are given as,

$$\Psi_g^{Ni} = \alpha_0|d^8> + \beta_0|d^9L> + \gamma_0|d^{10}L^2> . \tag{2}$$

$$\Psi_g^{Mn} = \alpha_0|d^3> + \beta_0|d^4L> . \tag{3}$$

The ligand-metal charge transfer energy is defined as, Δ=E($d^{n+1}L$)-E(d^n)(ie $<d^n|\mathrm{H}|d^n>$-$<d^{n+1}L|\mathrm{H}|d^{n+1}L>$), where H is the model Hamiltionian describing the ground and excited states as mentioned by Okada *et al.* [15]. The $d^{n+2}L^2$ state occurs at a much higher energy, given by E($d^{n+2}L^2$)-E(d^n)=$2\Delta+U_{dd}$, where U_{dd} = E(d^{n-1})+E(d^{n+1})-2E(d^n) is the d-d Coulomb interaction[15]. The off-diagonal matrix elements viz. $V = <d^n|\mathrm{H}|d^{n+1}L> = <d^nL|\mathrm{H}|d^{n+2}L^2>$ which are the one-electron transfer integrals correspond to the metal-ligand hybridization.

The anisotropy in V due to splitting between the t_{2g} and e_g states in Ni and Mn are represented as V_{e_g} and $V_{t_{2g}}$ respectively. In our calculations, $V_{t_{2g}}$ is fixed at 1 eV, thus V_{e_g} is the single adjustable parameter. The hybridizations strengths are related to Slater-Koster transfer integrals ie V_{e_g} = -$\sqrt{3}V_{pd\sigma}$ and $V_{t_{2g}}$ =-$2V_{pd\pi}$[16]. The final states involves effect of $2p$ core hole which reduce final state energies by a constant term U_{dc}. The ratio U_{dd}/U_{dc} was varied between 0.8 and 0.9 for optimum matching between experimental and calculated spectra. In the case of $2p$ XPS spectra the final states are,

$$\Psi_f^{Ni} = \alpha|\underline{c}d^8> + \beta|\underline{c}d^9L> + \gamma|\underline{c}d^{10}L^2> . \tag{4}$$

$$\Psi_f^{Mn} = \alpha|\underline{c}d^3> + \beta|\underline{c}d^4L> . \tag{5}$$

In the case of $2p$ XAS, the final states which are of the type $2p^53d^{n+1}$ are given by,

$$\Psi_f^{Ni} = \alpha_1|\underline{c}d^9> + \beta_1|\underline{c}d^{10}L> . \tag{6}$$

$$\Psi_f^{Mn} = \alpha_1|\underline{c}d^4> + \beta_1|\underline{c}d^5L> . \tag{7}$$

In the above equations $\underline{c}$ denotes the core-hole wavefunction. The calculations were done for the full multiplet spectrum[15]. The $3d-3d$ and $2p-3d$ Slater integrals were reduced to 80% of the Hartree-Fock values. Our XPS and XAS simulation involves three main parameters viz Δ, V and U_{dd}. The effect of bare crystal field splitting between the t_{2g} and e_g states were also included in the calculation by varying the separation $10Dq$ between 0 to 2.5 eV. The intensity of XPS and XAS spectra are calculated using sudden approximation[3, 15]. The defenition of Δ and U_{dd} are based on the centre of gravity of multiplet of each charge transfer configuration while the actual values of the two parameters are w.r.t the lowest energy of each configuration. These are appropriately labelled as Δ_{eff} and U_{eff}, both of which play a major role in determining the ground state electronic properties of the system.

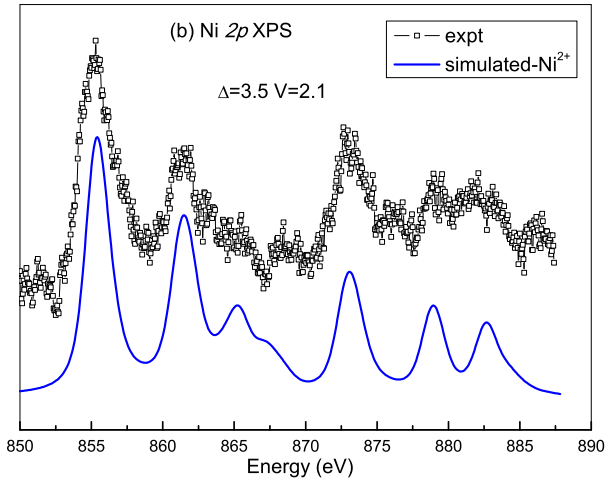

Figure 4. *Ni 2p XPS spectrum of Pr_2NiMnO_6 along with simulated spectra. The scales have been shifted for clarity.*

4.1.3. Ni 2p XPS spectra In Fig. 4, we show the Ni $2p$ XPS spectra of Pr_2MnNiO_6. The spectra shows spin-orbit split $2p_{3/2}$ and $2p_{1/2}$ regions with the main peaks located at 855 and 875 eV, respectively. Both the $2p$ regions contains two additional satellite features in addition to the main peak. The second satellite of the $2p_{3/2}$ is less prominent and has a lower intensity as compared to both the satellite peaks of $2p_{1/2}$. The second satellite of $2p_{1/2}$ is considerably broadened. The Ni^{2+} ion in Pr_2MnNiO_6 is surrounded by oxygen octahedra, similar to that in NiO. However the XPS spectra of NiO shows only a single satellite peak at each edge, which is seen in the bulk as well as thin films of NiO [2, 3, 17]. The second satellite feature is prominently seen nickel dihalide compounds, $NiCl_2$ and $NiBr_2$ while NiF_2 shows only a single satellite peak[3, 18]. The prominent appearance of the second satellite clearly indicates a reduced charge transfer energy and a greater covalency. Among the Ni dihalides, NiF_2 has the largest value of Δ due to the high electronegativity of fluorine, while Δ is smallest in the case of NiI_2.

The simulated Ni $2p$ XPS spectra for an NiO_6 cluster is shown in fig. 4. The spectra was optimised for $\Delta = 3.5$ eV and the hybridization ratio $V_{e_g}/V_{t_{2g}} = 2.1$ eV to match with the experimental spectrum. The values of U_{dd} and U_{dc} were 7.5 and 9.0 eV respectively. The higher values of U_{dd} are in agreement with the greater charge transfer character of the Ni^{2+} systems. From the relative values of Δ, U_{dd} and U_{dc}, the ground states and final states of the XPS spectra can be classified in four regimes [3]. In the case of our material since, $\Delta > 0$, the ground state has the following energy level sequence, $E(d^8) < E(d^9L) < E(d^{10}L^2)$. As the three parameters satisfy the following inequalities, $2\Delta + U_{dd} < U_{dc}$ and $U_{dc} - U_{dd} < \Delta < U_{dc} - U_{dd}/2$, in the final state, the level energy level sequence becomes $E(cd^9L) < E(cd^{10}L^2) < E(cd^8)$. Thus in fig. 4, the main peak has a majority cd^9L character while the first and second

satellite peaks belong to $cd^{10}L^2$ and cd^8 characters. The position and intensity of the satellites are dependent on the ratio of Δ/V. The weights of the d^8, d^9L and $d^{10}L^2$ components in the ground state are 0.78701, 0.20697 and 0.00603 respectively, which yields the average electron number $<n_d> = 8.21$ in the ground state. Using the relation mentioned by Fujimori *et al.* [19], we have determined Δ_{eff} and U_{eff}, which which are mentioned in table I. We find that $\Delta_{eff}>\Delta$ and $U_{eff}<U$ as seen in the late transition metal compounds. Thus analysis of Ni $2p$ XPS spectra suggests that the Ni-O bond in Pr_2MnNiO_6 has an intermediate covalent character.

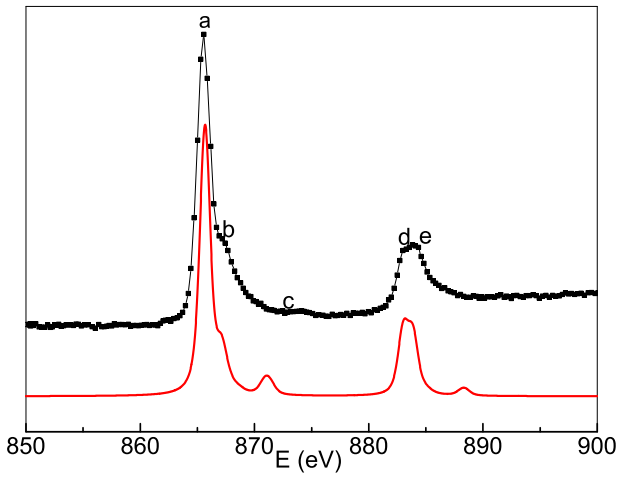

Figure 5. *Ni 2p absorption spectra of Pr_2NiMnO_6 along with simulated spectra.*

4.1.4. Ni 2p XAS The Ni $2p$ absorption spectra shown in Fig. 5, is split due to spin-orbit coupling into two main peaks $2p_{3/2}$ and $2p_{1/2}$. The spectra clearly displays characteristic feature of an Ni^{2+} system[20]. Compared to the XPS spectra, the satellite intensities are weaker. The absorption spectra contains distinct features marked a to f as shown in fig. 5. The separation between the main peak a and the shoulder peaks b and c and also the shape of the peaks are affected by Δ and V. Similar to the XPS spectra, the XAS spectra also is qualitatively similar to that of $NiBr_2$ and $NiCl_2$[20]. In fig. 5 we also show the simulated Ni^{2+} XAS spectra, which was obtained for $\Delta = 3.5$ eV and $V = 2.1$ eV. Unlike the XPS spectra, we have assumed only a single charge transfer configuration d^9L in the ground state since the $3d$ states becomes filled. The spectra was broadened by convoluting the line spectra with a Lorentzian function (0.3 eV) and Gaussian function (0.4 eV). The spectra also shows an additional broadening, especially for features b and c compared to that observed in the Ni dihalides. This can be attributed to the effect of presence of Ni^{3+} ions in the system due to random occupancies by Mn/Ni.

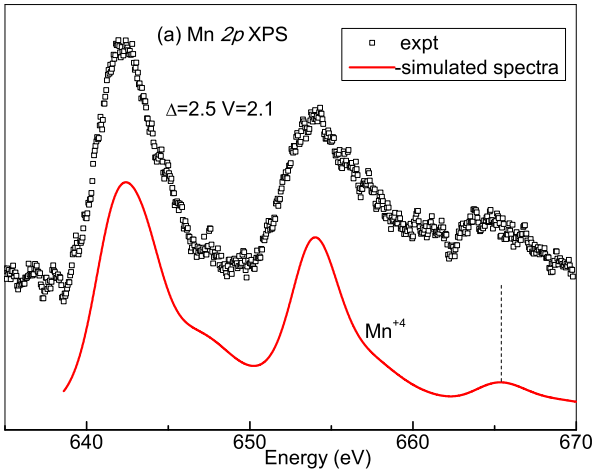

Figure 6. *Mn 2p XPS spectrum of Pr_2NiMnO_6 along with simulated spectra.*

4.1.5. Mn 2p XPS spectra In Fig. 6, we show the Mn $2p$ XPS spectra of Pr_2MnNiO_6. The spectra shows $2p_{3/2}$ and $2p_{1/2}$ spin-obit doublet peaks located at 642 and 654 eV, respectively. In addition we observe the satellite peak of $2p_{1/2}$, at a binding energy of 666 eV. The satellite peak of $2p_{3/2}$ is not visible since it overlaps with the $2p_{1/2}$ peak. The position of the satellite peak is sensitive to the d-electron number[21]. In fig.6 we also show the calculated Mn $2p$ spectra for an MnO_6 cluster. The calculated spectra is broadend with a energy dependent Lorentzian and Gaussian function of 0.5 eV each. The Mn spectra is broader compared to Ni due to greater multiplet splitting. The experimental spectra is well reproduced for Δ=2.5 eV and V=2.1 eV along with $U_{dd} = 6.5$ and and $U_{dc} = 8.5$ eV. Moroever the intensity of the satellite indicates that the system can be described by a pure Mn^{4+} configuration. Based on the values of the above four parameters, the main peak has a predominant cd^4L character while the satellite peak has cd^3L characters. Additional features indicating existence of Mn^{3+} ions is not so clearly seen in our XPS spectra. This is unlike the case of doped rare earth manganite systems where the satellite feature of the Mn $2p$ spectra can be expressed as a linear combination of Mn in 3+ and 4+ valence states[21]. The weights of the d^3, d^4L components in the ground state are 0.625 0.375 respectively, which yields the total electron number $<n_d> = 3.38$ in the ground state. Thus the higher d electron count than the ionic value of 3, arises due to the greater charge transfer character and hybridization of the MnO_6 cluster. The relatively smaller value of the charge transfer energy is comparable to the values obtained in isostructural Mn^{4+} systems viz. $CaMnO_3$ and $SrMnO_3$ [22].

4.1.6. Mn 2p XAS spectra The Mn $2p$ absorption spectra of Pr_2MnNiO_6 is shown in fig. 7. The spectra comprises of two main lines A and B corresponding to $2p_{3/2}$ and $2p_{1/2}$, without any additional satellite features. The spectral feature is similar to that

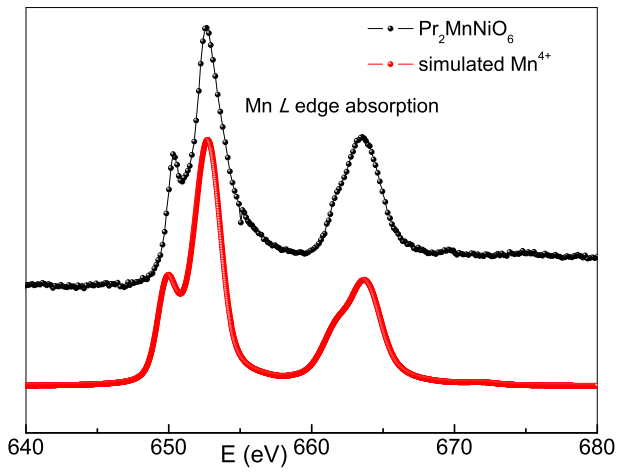

Figure 7. *Mn $L_{3,2}$ absorption spectra of Pr_2NiMnO_6 along with simulated spectra.*

Table 1. Best fit parameters obtained from Ni and Mn 2*p* XPS and XAS spectra for Pr_2MnNiO_6.

Compound	Ni	Mn
Δ	3.5	2.5
Δ_{eff}	4.5	1.5
U_{dd}	7.5	6.5
U_{eff}	5.5	6
n_d	8.21	3.38
$V_{e_g}/V_{t_{2g}}$	2.1	2.0
$V_{pd\sigma}$	1.21	1.2

of Mn^{4+} as observed in $CaMnO_3$ without any sign of Mn^{3+} feature. Unlike the Mn 2*p* XPS spectra, the XAS spectra does not show any distinct satellite features due to charge transfer configurations. The Mn 2*p* XAS spectrum is also theoretically simulated assuming a d^3 electronic configuration with t_{2g}^3 ($^4A_2$) symmetry in the ground state. However the Mn 2*p* absorption spectra is highly sensitive to the crystal field splitting $10D_q$, unlike the XPS spectra. The feature at 650 eV corresponds to the crystal field splitting. The experimental spectra is successfully reproduced for $10D_q$ = 2.4 eV. This value is similar to that used for simulation in the case of $La_{0.9}Ca_{0.1}MnO_3$, which is predominantly an Mn^{4+} system[23].

4.2. O K edge and density of states

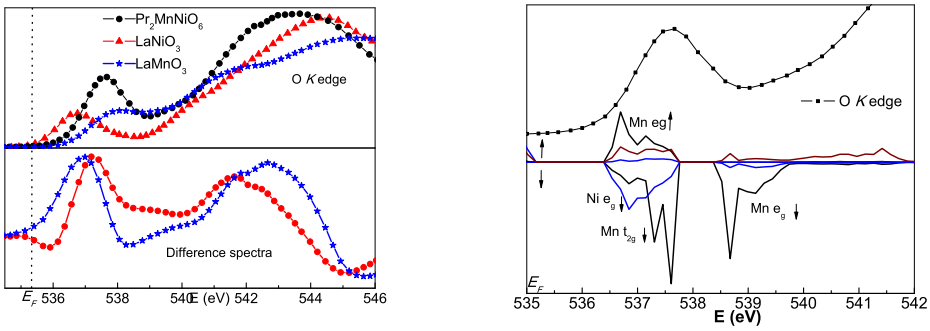

Figure 8. *a*The 0 K-edge absorption spectra of Pr_2NiMnO_6, along with $LaNiO_3$ and $LaMnO_3$(upper panel). The fermi energy is marked with rising edge of metallic $LaNiO_3$. Lower panel contains the difference spectra of Pr_2NiMnO_6 obtained by subtracting the two parent compounds. (b) Enlarged pre-edge of Pr_2NiMnO_6 highlighting the Mn(Ni)3d-O2p hybridized unoccupied states and corresponding density of states above Fermi energy for $U-J=$ 2 eV.

Fig. 8a(upper panel) shows the normalized O K edge spectra of Pr_2MnNiO_6 collected in the total electron yield mode. The first prominent peak of the (536-539 eV) spectra arises due to the transition from O 1s state to unoccupied O 2p states. These states occur due to hybridization between the O 2p and 3d states of Mn and Ni above the Fermi energy(E_F). For determination of E_F, we also present normalized spectra of $LaNiO_3$, which is metallic compound. We also show the spectra of $LaMnO_3$, which has a known band gap. The Fermi energy was obtained by the rising edge of $LaNiO_3$ as shown in fig. 8a. The rise in spectra of $LaMnO_3$ occurs around 1.1 eV above E_F, which can thereby be considered as its bandgap, which close to the bandgap of 1.2 eV obtained from optical conductivity measurements[24]. For comparision of the spectra of the three compounds, normalization was done at the post edge above 570 eV, which corresponds to a continuum. Based on the rising edge of our compound (10% of peak intensity) we estimate a bandgap of nearly 0.9 eV for Pr_2MnNiO_6, which is around 0.5 eV greater than the value obtained from resistivity measurements. However the band gap is much lower than the reported value of 1.4 eV in the case of La_2MnNiO_6 thin films[25]. The experimental band gap is also affected by presence of anti-site disorders, which are insulating regions.

The first peak in Pr_2MnNiO_6 occurs around 2.5 eV above E_F as seen in fig. 8a. The peak intensity is almost twice that of $LaNiO_3$ and $LaMnO_3$. The large intensity arises due to the larger amount of unoccupied states of Mn^{4+} ion, along with unoccupied states from Ni^{2+} ion. However the intensity is also affected by the covalency between the Mn-O and Ni-O which is much higher for an Mn^{4+} system. An indirect measure of covalency in the ground state is the intensity of the pre-peak edge in the O 1s spectra which is roughly proportional to β_0^2[4]. The large intensity of the O 1s pre-peak edge at 537 eV indicates a greater covalent character of our system as compared to compared to $LaMnO_3$. This is also valid in the case of O K edge of $PrMnO_3$[26], since in $RMnO_3$

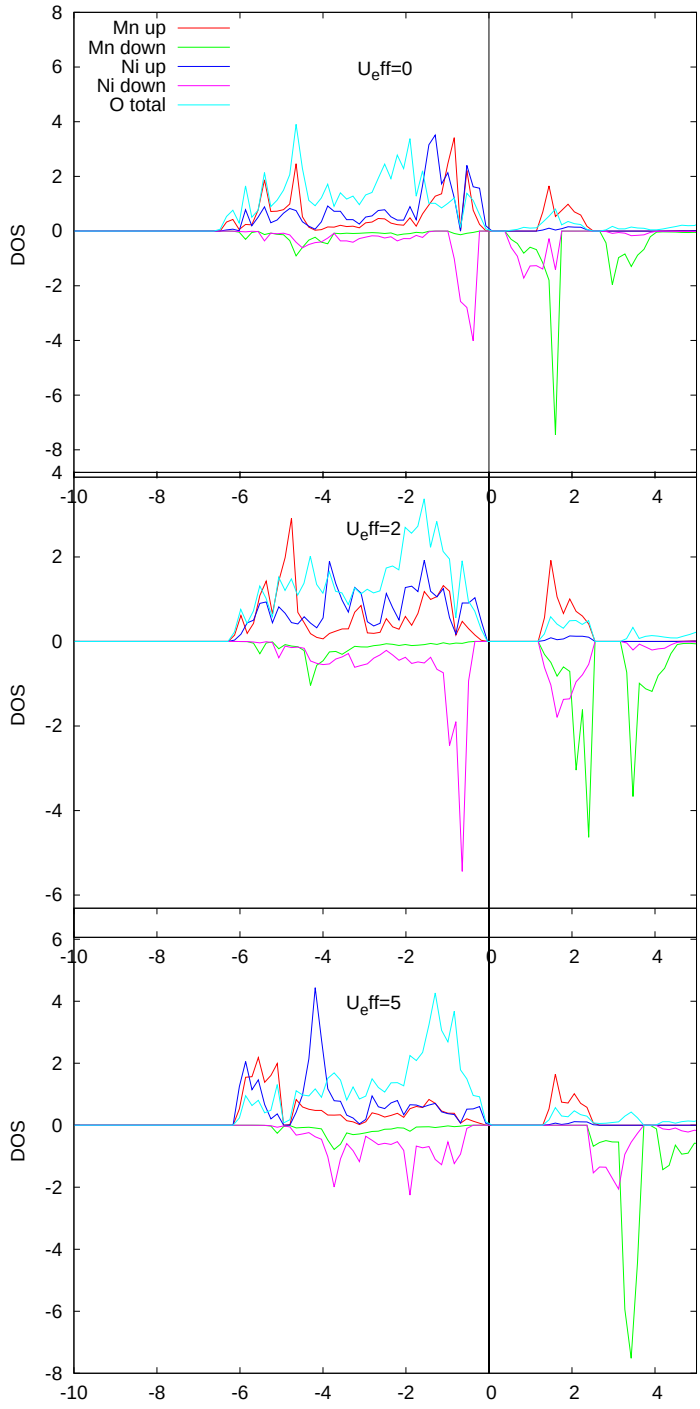

Figure 9. *Spin polarized local density of states per formula unit of Pr_2MnNiO_6 for Mn and Ni 3d states and O 2p states for (a) $U_{eff} = 0$ eV, (b) 2 eV and (c) 5 eV, where $U_{eff} = U - J$. The zero is the Fermi energy E_F.*

increase in R does not drastically affect the covalency character and the bandgap. The combined effect of the Ni and Mn 3d states above E_F in Pr_2MnNiO_6 is seen from our difference spectra w.r.t $LaNiO_3$ and $LaMnO_3$, which is shown in lower panel of fig.8a. The difference spectra w.r.t $LaNiO_3$ shows an initial dip just above E_F, which indicates depletion of states above E_F due to non-zero band gap. Above 536 eV we see emergence of the unoccupied states. The depletion region area is much smaller than the enhanced region. Similarly on comparision with $LaMnO_3$, we see a large increase in the unoccupied states. The major contribution to the spectral intensity arises from the unoccupied Mn e_g ($\uparrow$ and $\downarrow$) and t_{2g} $\downarrow$ states while a smaller contribution arises from the Ni e_g $\downarrow$ states. Thus the large enhancement of the unoccupied states above E_F indicating large overlap between the Mn 3d and Ni 3d bands in Pr_2MnNiO_6.

Fig. 9 shows the spin resolved partial density of states of Pr_2MnNiO_6 comprising of the 3d states of Mn and Ni along with O 2p states for three values of $U-J$ viz. 0, 2 and 5 eV. The Ni and Mn the 3d states split into t_{2g} and e_g states due to crystal field splitting. Below E_F, the spin up channel is occupied by the Mn $t_{2g}\uparrow$ along with Ni $t_{2g}\uparrow$ and partially filled $e_g\uparrow$ states. We observe that below -2 eV the O 2p states contribute significantly to the density of states. The Ni e_g states occur close to the Fermi energy in the range 0 to -1 eV with a peak at -0.8 eV. On the other hand the Ni t_{2g} shows a prominent peak at -1.2 eV.

Above the Fermi energy, the Mn $e_g\uparrow$ states dominate the spin-up channel occuring at around 1.5 eV above E_F. However the the Mn $t_{2g}\downarrow$ states from the spin-down channel are closer to E_F(+0.5 eV). This shows a strong overlap with the Ni $e_g\downarrow$ states. The spin down channel below E_F is dominated by the Ni $t_{2g}\downarrow$ states. From our first principles calculations, the the Mn moments show a value of $2.8\mu_B$ while the Ni moments show a lesser value of $1.4\mu_B$. The theoretical values are lower than the atomic values of $3\mu_B$ and $1.9\mu_B$. The reduction in the values can be attibuted to the greater delocalization of the Ni states.

The density of states show sufficient mixing between the Mn and Ni states near the Fermi energy. In the absence of U, the system shows a band gap of 0.5 eV which is similar to the values obtained in La_2MnNiO_6[27]. This is unlike the parent manganites which show a ferromagnetic metallic ground state in the absence of correlations. Thus the overlap of Ni and Mn 3d states, causes a drastic reduction in band gap compared to that of $CaMnO_3$ or NiO which are isovalent compounds. The effect of U is more complex due to the inequivalent nature of the two transition metal atoms. To probe the effect of correlations, the calculations were also performed for different values of U-J ie 2, 5 and 8 eV. With increase in U,the O 2p states increase in intensity, just below the Fermi energy. Also for $U = 2$ has a higher band gap of 1 eV, which remains constant even at 8 eV(not shown). However with increase in U, there occurs a shift in Ni and Mn 3d states which become highly localized. The constant band-gap indicates absence of a prominent effect of further increase in U especially on the Mn $e_g\uparrow$ states above E_F. This is unlike the parent manganites, in which show a greater increase in band gap with increase in U in a systematic manner. Since the O K edge is a direct representation of the unoccupied DOS, we compare the Mn 3d, Ni 3d and O 2p DOS in fig. 8b. The nature of spectra qualitatively for $U-J = 2$ eV since for this value we obtain a band gap of approximately 0.9 eV which is comparable to the rising edge of O K edge spectra. Based on the DOS the O K pre-peak can be divided into two portions. The first part comprises of the strongly overlapping Mn $e_g\uparrow$ and Ni $e_g\downarrow$ states. The large rise in the central portion can be attributed entirely to the Mn $t_{2g}\downarrow$ states while the subsequent edge arises due to the Mn $e_g\downarrow$ states. However unlike in

parent manganite compounds, there is no effect of U on Mn $e_g\uparrow$ states.

4.3. Role of charge transfer, covalency in band gap

In Pr_2MnNiO_6, the Ni^{2+} ion unlike in NiO has smaller charge transfer energy due to which the d^9L state has significent occupancy. Similarly, the d^3 states are strongly hybridized to the d^4L states in the Mn^{4+} ion. The band gap of the material is determined by interplay of U_{dd}, Δ and V, the later two reflecting the degree of covalency between the Ni-O and Mn-O bonds. An estimate of the hybridization strength is obtained from the Slater-Koster method, by finding the Ni(Mn) $3d$-O $2p$ transfer integral $V_{pd\sigma} \sim \beta_0 \sim 1/d^{3.5}$, where d corresponds to the average Ni-O and Mn-O bond lengths. The average Ni-O and Mn-O bond-lengths in Pr_2MnNiO_6 which are 2.04 and 1.9Å respectively yield $V_{pd\sigma} = 1.13$ eV for Ni-O and a much higher value of 1.8 eV for Mn-O bonds respectively. Thus the bare hybridization strength is much greater for Mn-O bonds as compared to the Ni-O bonds. However the cluster analysis of $2p$ XPS spectra yield nearly equal value, $V_{pd\sigma} = 1.21$ eV for both the ions. In case of Ni^{2+} ion, $V_{pd\sigma}$ is comparable to the value of bare Slater-Koster integral, and also compares to the value obtained for NiO from cluster analysis[16]. However in the case of Mn we see a considerable reduction in $V_{pd\sigma}$, when compared to values obtained for $SrMnO_3$ and $CaMnO_3$. For both these compounds, $V_{pd\sigma}$ is in the range betweem 1.5 and 1.6 eV, as obtained from XPS and XAS spectra[6, 21].
Thus $CaMnO_3$ and $SrMnO_3$ with a much smaller Δ_{eff} show a strongly hybridized ground state due to which they are considered as charge transfer insulators. In the case of parent $LaMnO_3$, a large value of 2.2 eV is obtained for $V_{pd\sigma}$, but due to relatively higher value of Δ_{eff} the $RMnO_3$ compounds have a mixed character, ie between that of a Mott-Hubbard and charge transfer insulator in the ground state[28].
At the other extreme, in the case of $RNiO_3$, the scenario is entirely different. Based on the average Ni-O bondlength of 1.94Å, bare hybridization strength yields a value of 0.9 eV in $PrNiO_3$. However the cluster calculation yields a ground state with large value of $\beta^2 \sim 0.55$ and $V_{pd\sigma} = 1.5$ eV, which is much greater than the bare Slater-Koster transfer integrals. The large covalency due to a small transfer energy ($\Delta \sim 1$ eV) and a large inter-cluster hopping strength due to Ni-O-Ni bonds are responsible for the metallicity in $LaNiO_3$[29]. The apparent increase in Ni-O bond length and reduction in Ni-O-Ni bond angles from La to Nd drastically affect the hopping integrals and the e_g bandwidth[30]. This results in a transition from metallic to insulating state with a very small band gap in $PrNiO_3$ and $NdNiO_3$. Thus $PrNiO_3$ and $NdNiO_3$ are considered as "covalent insulators" which are intermediate between charge transfer insulator and $p-d$ metal in the ZSA diagram [30]. However in the case of $RMnNiO_6$ the changes in Mn(Ni)-O bond lengths and Mn-O-Ni bond angles do not affect the band width of the e_g orbitals, even though changes in super-exchange strength thereby reduces the transition temperatures. The Mn-O-Ni hopping integrals are not much affected by small changes in bond lengths and bond angles. This is also seen indirectly from high pressure studies on La_2MnNiO_6 which retains its ferromagnetic character even under 30 GPa pressure, with a small variation in T_C and reduction in magnetic moments[31]. Thus in the $RMnNiO_6$ double perovskites the charge transfer and overlap of Mn^{4+} with oxygen and Ni^{2+} ions have a more robust character due to which the bandgap remains largely unaffected.

Based on the scheme of ZSA diagram, the Ni^{2+}-based compounds(except NiO), the band gap in terms of the simple charge transfer model can be expressed as,

$E_g = \Delta+\delta$-$W/2$; where W corresponds to the ligand band-width, and δ=$2\delta^n$-δ^{n-1}-δ^{n+1}, corresponds to lowering of energy of $3d^8$ configuration due to hybridization[1]. In a simplified approximation, the band gap E_g is given by Δ_{eff}-W, where W=$(W_p+W_d)/2$, is the average of the cation and anion bandwidths[19]. From the SIAM model, we can assume that $W_p = 4$ eV and $W_d = 0.5$ eV (for Ni and Mn $3d$ bandwidths). Thus if we consider Δ_{eff} of Ni^{2+} alone in Pr_2MnNiO_6, we would obtain a band gap of 2.25 eV, which though smaller than NiO by half still is much greater than the experimental value of 0.8 eV. In the present scenario the highly reduced Δ_{eff} of Mn results in a net metal-ligand charge transfer energy which can be considered as average between values of Mn and Ni. Thus considering $\Delta^{av}_{eff} = 3$ eV, we obtain a band band gap of 0.75 eV, which is much closer to the experimentally obtained values, thereby suggesting a net-charge transfer effect. The effect of charge transfer nature is also seen from the DOS in fig. 9. At U=0 eV, since the highest spectral weight is of $3d$, the gap is of $d-d$ type. With increase in U, there is a large shift in spectral weight from $3d$ to O $2p$ states. Thus from first princples along with XPS studies it is seen that the the band gap of Pr_2MnNiO_6 is of $p-d$ type with an intermediate covalent character.

4.4. Conclusions

To summarize, the electronic structure of double perovskite compound Pr_2MnNiO_6 is studied using $2p$ core XPS and XAS along with O K edge absorption. The Ni $2p$ XPS shows a three peak structure indicating a greater charge transfer effect. Using the charge transfer multiplet theory it is found that Ni^{2+} has a lower charge transfer energy of 3.5 eV as compared to NiO compound resulting in a ground state of Ni is 78% d^8, 21% d^9L and 0.6% d^9L^2. Similar analysis of Mn $2p$ XPS reveal that Mn^{4+} has a charge transfer energy of 2.5 eV, which is close to that of $CaMnO_3$ and $SrMnO_3$. The ground state of Mn is 62% d^3 and 38% d^4L. The ground state of Ni^{2+} and Mn^{4+} reveal a much higher d electron count of 8.21 and 3.38 respectively. Based on our cluster analysis, we estimate a band gap of 0.75 eV which is close to the value obtained from the O K edge spectra. Since for Mn^{4+} and Ni^{2+}, U>Δ and U_{eff}>Δ_{eff} conditions are satisfied, Pr_2MnNiO_6 can be considered as a charge transfer insulator, with an intermediate covalent character. The density of states reveal a band gap of nearly 1 eV for $U-J$>0, and remains constant even for $U-J$=8 eV. Similarly our density functional theory calculations show that the band gap is of p-d type confirming the more robust charge transfer nature.

5. References

[1] Zannen J, Sawatzky G and Allen J 1985 *Phys. Rev. Lett.* **55** 418
[2] Bocquet A, Mizokawa T, Matoba M and S A 1995 *Phys. Rev. B.* **52** 13838
[3] Zannen J, Westra C and Sawatzky G 1986 *Phys. Rev. B.* **33** 8060
[4] Medarde M, Fontaine A, Garcia-Munoz J, Rodriguez-Carvajal J, Santis M, Sacchi M, Rossi G and Lacorre P 1992 *Phys. Rev. B.* **46** 14975
[5] Pickett W E and Singh D J 1996 *Phys. Rev. B.* **53** 1146
[6] Saitoh T, Bocquet A E, Mizokawa T, Namatame H, Fujimori A, Abbate M, Takeda Y and Takeda Y 1995 *Phys. Rev. B.* **51** 13942
[7] Joly V, Joy P, Date S and Gopinath C 2002 *Phys. Rev. B* **65** 184416
[8] Dass R, Yan J Q and Goodenough J 2003 *Phys. Rev. B.* **68** 064415
[9] Booth R, Fillman R, Whitaker H, Nag A, Tiwari R, Ramanujachary K, Gopalakrishnan J and Lofland S 2009 *Mater. Res. Bull.* **44** 1559–1564
[10] Shi C, Hao Y and Hu Z 2011 *J. Phys. D. Appl. Phys.* **44** 245405

[11] Galakhov V R, Demeter M, Bartkowski S, Neumann M, Ovechkina N A, Kurmaev E Z, Lobachevskaya N I, Mukovskii Y M, Mitchell J and Ederer D L 2002 *Phys. Rev. B.* **65** 113102
[12] Kresse G and Furthmüller J 1996 *Physical review B* **54** 11169
[13] Van Vleck J 1934 *Phys. Rev.* **45** 405
[14] deGroot F 2005 *Coordination Chemistry Reviews* **249** 31
[15] Okada K and Kotani A 1992 *J. Phys. Soc. Japan.* **61** 4619
[16] Bocquet A, Mizokawa T, Saitoh T, H N and A F 1992 *Phys. Rev. B.* **46** 3771
[17] Alders D, Voogt F, Hibma T and Sawatzky G 1996 *Phys. Rev. B* **54** 7716
[18] Okada K and Kotani A 1991 *J. Phys. Soc. Japan.* **60** 772
[19] Fujimori A, Bocquet A, Saitoh T and Mizokawa T 1993 *J. Elec. Spect. Rel. Phen.* **62** 141
[20] van der Laan G, Zannen J, Sawatzky G, Karnatak R and Esteva J M 1986 *Phys. Rev. B.* **33** 4253
[21] Zampieria G, Pradoa F and Caneiroa A 2002 *Sol. Stat. Comm.* **123** 81
[22] Park J H, Chen C, Cheong S W, Bao W, Meigs G, Chakarian V and Idzerda Y 1996 *Phys. Rev. Lett.* **76** 4215
[23] Abbate M, de Groot F, Fuggle J, Fujimori A, Strebel O, Lopez F, Domke M, Kaindl G, Sawatzky G, Takano M, Takeda Y, Eisaki H and Uchida S 1992 *Phys. Rev. B* **46** 4511
[24] Jung J H, Kim K H, Eom D J, Fujimori A, Noh T W, Choi E J, Jaejun Y, Kwon Y S, Kwon Y S and Chung Y 1997 *Phys. Rev. B* **55** 15489
[25] Lan C, Zhao S, Xu T, Ma J, Hayase S and Ma T 2015 *J. Alloys. Compounds.* **655** 208
[26] Toulemonde O, Millange F, Studer F, Raveau B and Park J H 1999 *J. Phys. Cond. Mat.* **11** 109
[27] Das H, Waghmare U V, Saha-Dasgupta T and Sarma D D 2008 *Phys. Rev. Lett.* **100** 186402
[28] Chainani A, Mathew M and Sarma D 1993 *Phys. Rev. B.* **47** 15397
[29] Barman S, Chainani A and Sarma D 1994 *Phys. Rev. B.* **49** 8475
[30] Sarma D D, Shanti N and Mahadevan P 1994 *J. Phys. Cond. Mat.* **6** 10467
[31] Haskel D, Fabbris G, Souza-Neto N M, Veenendaal v M, Shen G, Smith A E and Subramanian M A 2011 *Phys. Rev. B* **84** 100403